Title: Efferocytosis-Driven M2 Macrophage Impairs Fibrotic Encapsulation and Promotes *Echinococcus multilocularis* Growth in Cotton Rats (*Sigmodon Hispidus*)

Running head: M2 Macrophages and Parasite Growth in Cotton Rats

Authors: Maru Manabe[1,#], Teppei Nakamura[1,#,*], Keisuke Sato[1], Naoki Hayashi[2,3], Hirokazu Kouguchi[4], Ryo Nakao[2,3,5], Masahito Hidaka[4], Hiroyuki Matsuyama[4], Nariaki Nonaka[2,3,5], Masami Morimatsu[1]

Affiliations:

[1] Laboratory of Laboratory Animal Science and Medicine, Department of Applied Veterinary Sciences, Faculty of Veterinary Medicine, Hokkaido University, Sapporo, Hokkaido 060-0818, Japan

[2] Laboratory of Parasitology, Department of Disease Control, Faculty of Veterinary Medicine, Faculty of Veterinary Medicine, Hokkaido University, Sapporo, Hokkaido 060-0818, Japan

[3] Division of Parasitology, Veterinary Research Unit, International Institute for Zoonosis Control, Hokkaido University, Sapporo, Hokkaido 001-0020, Japan

[4] Medical Zoology Group, Department of Infectious Diseases, Hokkaido Institute of Public Health, Sapporo, Hokkaido, 060-0819 Japan

[5] One Health Research Center, Hokkaido University, Sapporo, Hokkaido 060-0818, Japan

# equal contribution

***Corresponding author**: Teppei Nakamura, DVM, PhD

Laboratory of Laboratory Animal Science and Medicine, Department of Applied Veterinary

Sciences, Faculty of Veterinary Medicine, Hokkaido University, Sapporo, Hokkaido 060-0818, Japan

Tel: +81-01-706-5107, E-mail: nakamurate@vetmed.hokudai.ac.jp

Abstract

Alveolar echinococcosis, caused by *Echinococcus multilocularis*, exhibits significant species-dependent susceptibility. This study compared the early hepatic tissue responses to *E. multilocularis* in highly susceptible cotton rats (*Sigmodon hispidus*) and laboratory mice (DBA/2 and AKR/N). Following oral administration of *E. multilocularis* eggs, cotton rats developed a greater number of hepatic lesions within two weeks, whereas mice required four weeks to develop smaller lesions. Histopathology revealed accelerated multilocular cyst formation in cotton rats. Unlike mice, which formed dense collagenous layers isolating cysts, cotton rats lacked adventitial layers despite similar fibrotic thickness. Immunohistochemistry revealed abundant $CD206^{+}$ macrophages at cyst peripheries in cotton rats, engaging in efferocytosis of apoptotic neutrophils with expression of TGF-β, galectin-3, and VEGF. Efferocytic macrophages expressed collagen-degrading enzymes (cathepsin K and MMP9) and the growth factor FGF2. These findings suggest that efferocytosis by neutrophils drives macrophages toward an anti-inflammatory M2 phenotype, leading to immune evasion, ineffective fibrotic encapsulation, and parasitic growth. Given the wide distribution of cotton rats in the Americas and the expanding range of *E. multilocularis*, their hypersusceptibility raises significant public health concerns as rodents could serve as an intermediate host. These insights may inform new strategies for host-parasite interactions and the control of alveolar echinococcosis.

Key words: *Echinococcus multilocularis*, Cotton rat, Macrophage polarization, Efferocytosis , Fibrosis

INTRODUCTION

Echinococcosis is a parasitic disease caused by a cestode of the genus *Echinococcus* and is primarily classified into cystic and alveolar echinococcosis. The latter, caused by *Echinococcus multilocularis*, is distributed across a wide range of parts of the Northern Hemisphere, including Central Asia, China, Europe, and Russia (Díaz et al., 2011; Torgerson et al., 2010), and has recently raised public health concerns in North America (Massolo et al., 2014). *Echinococcus multilocularis* maintains its life cycle between canids (e.g., foxes and dogs) as definitive hosts and rodents as intermediate hosts. Humans and pigs serve as accidental intermediate hosts that are infected through the ingestion of parasite eggs (Díaz et al., 2011; Torgerson et al., 2010). In humans, alveolar echinococcosis can lead to severe hepatic complications. In advanced cases, the parasite disseminates to extrahepatic organs such as the lungs, brain, and spleen, leading to poor clinical outcomes if left untreated (Torgerson et al., 2010). Adult parasites reside in the small intestine of definitive hosts and release eggs that are excreted in feces. When ingested by intermediate hosts, the eggs hatch into oncospheres that penetrate the intestinal wall and migrate via the portal vein to the liver, where they enter the metacestode stage (Hayashi et al., 2021). Larval cysts develop through several stages: formation of unilocular cysts, multilocularization, development of the laminated layer, and formation of brood capsules and protoscoleces (Sakamoto & Sugimura, 1970). Host–parasite interactions critically influence disease progression. The laminated layer produced by the parasite facilitates immune evasion, whereas early deposition of host-derived connective tissue may help protect larvae from immune attacks (Vuitton et al., 2006).

Among various animal models that have been employed to elucidate the factors influencing *E. multilocularis* infection, rodents are indispensable for dissecting infection mechanisms. While most laboratory mouse strains (e.g., C57BL/6 and BALB/c) display resistance, DBA/2 and AKR mice show higher susceptibility (Matsumoto et al., 2010; Nakaya

et al., 1997). Strain differences revealed distinct polygenic factors contributing to larval cyst establishment and subsequent protoscolex development (Nakao et al., 2011). Mouse models have also highlighted macrophages as the central regulators of the host immune response during infection. Macrophages play key roles in tissue homeostasis including foreign body clearance, fibrosis, and wound healing (Wynn & Vannella, 2016). Upon activation, they polarize into M1 (pro-inflammatory) or M2 (anti-inflammatory) subsets, both of which are involved in regulating inflammation and fibrogenesis (Jiang et al., 2024). In the context of *E. multilocularis* infection, M1 macrophages are thought to contribute to early larval clearance, whereas M2 macrophages are associated with persistent infection and fibrotic encapsulation (Wang et al., 2021).

The susceptibility to *E. multilocularis* infection also varies among different species. Cotton rats (*Sigmodon hispidus*; Cricetidae) represent a uniquely hypersusceptible model that develops multilocular cysts within two weeks of egg inoculation, which is much faster than in susceptible mouse strains (Matsumoto et al., 2010). Notably, wild cotton rats inhabit grasslands across the southern United States through Mexico, Central America, and northern South America, overlapping with the expanding geographic range of *E. multilocularis* in North America (Faith et al., 1997; Massolo et al., 2014). If the parasite establishes its life cycle using cotton rats as intermediate hosts, it poses a serious public health risk. Understanding the mechanisms underlying the hypersusceptibility of cotton rats to *E. multilocularis* will provide critical insights for predicting transmission dynamics, developing targeted surveillance strategies, and preventing the expansion of *E. multilocularis* in North and South America.

Given that macrophages serve as key effector cells in the pathogenesis of *E. multilocularis* infection in both mice and cotton rats (Reuben et al., 1978; Wang et al., 2021), we hypothesized that macrophages, particularly those of the M2 subtype, play a central role in facilitating early parasite establishment. This study aimed to elucidate the mechanisms of hypersusceptibility to *E. multilocularis* in cotton rats by comparing their liver histopathology with that in mice.

MATERIALS AND METHODS

Animals

This study was performed in strict accordance with the National Institutes of Health Guide for the Care and Use of Laboratory Animals. The Ethics Committee of the Hokkaido Institute of Public Health approved the protocol for animal experiments (permit number: K22-1). Male inbred cotton rats maintained at the Hokkaido Institute of Public Health were used at 8 9 weeks of age when they were infected (n=5). Male DBA/2CrSlc and AKR/NSlc mice (n = 5 each), both susceptible to *E. multilocularis*, were used at seven weeks of age. Data from both the strains were combined to minimize strain bias.

Archived paraffin-embedded tissues from female cotton rat kidneys with tubulointerstitial fibrosis (11 months old) and juvenile male cotton rat livers (1 month old) were used (Ichii et al., 2016; Nakamura et al., 2019). These samples were used to evaluate antibodies for the detection of distinct M2 macrophage subsets in cotton rats.

Infection experiment of E. multilocularis

Echinococcus multilocularis of Nemuro strain was maintained and transferred to dogs and cotton rats at the Hokkaido Institute of Public Health. *Echinococcus multilocularis* eggs were collected from feces of experimentally infected dogs with *E. multilocularis* according to the method described previously (Kouguchi et al., 2016) and kept at 4 °C for about 3 months. Two hundred eggs were orally administered to each animal (n=5 each in cotton rats, DBA/2, and AKR/N). Cotton rats were dissected after 2 weeks, and mice were dissected after 4 weeks. The animals were euthanized by cutting their hearts under deep anesthesia with isoflurane. After gross observation, one white spot-like lesion was randomly selected from each of the two liver lobes per animal, and approximately 5 mm squares of the tissue including the lesions were

harvested.

Light microscopy

The livers were fixed in 10 % neutral-buffered formalin and embedded in paraffin. Semi-serial sections of 2 μm thickness were prepared at approximately 100 μm intervals. The sections were stained with hematoxylin and eosin (HE), periodic acid Schiff (PAS), Luna, and picrosirius red, and were subjected to immunostaining as described below. For Luna staining to detect eosinophil granules, the slides were immersed in a mixture of Weigert's iron hematoxylin and Biebrich scarlet for 10 min, differentiated in 1 % acid alcohol, and then dipped in 0.5 % lithium carbonate. For picrosirius red staining to visualize collagen fibers, the slides were immersed in Weigert's iron hematoxylin for 10 min and washed with tap water. Subsequently, they were immersed in 1 % acetic acid for 1 min, followed by immersion in 0.04 % Sirius Red in saturated picric acid for 10 min. At least five sections per liver samples were examined to determine the number and the developmental stages of *E. multilocularis* larval cysts according to the criteria established by Sakamoto et al., with minor modifications (Sakamoto & Sugimura, 1970). Stage 1: infiltration foci without larval cysts, indicating parasite elimination; Stage 2: unilocular cysts; Stage 3: multilocular cysts with internal septation; Stage 4: multilocular cysts with exogenous budding; Stage 5: brood capsule formation characterized by active proliferation of germinal cells. Since internal septation was consistently observed in cysts with exogenous budding, but not all septated cysts exhibited budding, we defined exogenous budding to represent a more developed stage. The presence of a cuticular layer was confirmed by PAS staining.

Immunohistochemistry and immunofluorescence

Details of the antibodies used are listed in Supplemental Table 1. For immunohistochemistry, sections were deparaffinized, heated for antigen retrieval, and treated

with 0.3 % hydrogen peroxide/ethanol solution for 30 min to eliminate endogenous peroxidase. The sections were treated with normal goat serum (Nichirei, Tokyo, Japan) for 30 min at room temperature, and incubated overnight with primary antibodies at 4 °C. The sections were then incubated with biotin-labeled secondary antibodies for 30 min, followed by treatment with streptavidin-peroxidase (Nichirei) for 30 min at room temperature. The immunopositive reactions were developed using a 3,3'-diaminobenzidine tetrahydrochloride-H_2O_2 solution. The sections were counterstained with hematoxylin.

For immunofluorescence, the sections were deparaffinized and subjected to heat-induced antigen retrieval. The sections were treated with 3 % BSA in PBS for 30 min at room temperature, and incubated overnight with primary antibodies at 4 °C. The sections were then treated with Alexa Fluor-labeled secondary antibodies for 30 min. The sections were counterstained with DAPI.

Histomorphometry

Images were captured using a BZ-X800 microscope (Keyence, Osaka, Japan) or NanoZoomer 2.0-RS (Hamamatsu Photonics, Shizuoka, Japan). Based on the picrosirius red staining, the thickness of the fibrotic region surrounding the larval cysts and the ratio of the Sirius red$^+$ area in the layer were measured using ImageJ (version 1.54p, National Institutes of Health, MD, USA). To evaluate the distribution of CD163$^+$, CD206$^+$, and ssDNA$^+$ cells, the area surrounding the cysts was divided into three layers: pericystic, fibrotic, and uninfected liver regions. The area and the number of positive cells per unit area were calculated.

Statistical analysis

Data are presented as mean ± standard error. Statistical analyses were performed using unpaired *t*-tests for two groups and one-way ANOVA with Tukey's multiple comparison test for

three groups.

RESULTS

Gross observation of infected liver

Four weeks after egg inoculation, white foci were diffusely distributed in the liver of four out of five DBA/2 mice and in all AKR/N mice (Figs. 1A and B). In contrast, scattered white foci were observed in the livers of cotton rats two weeks after egg inoculation (Fig. 1C). The foci in cotton rats were approximately 0.5 to 2 mm in diameter, while those in mice ranging from 0.7 mm to 1 mm in diameter.

Histology of infected liver

Larval cyst development progressed more rapidly in cotton rats than in the susceptible mouse strains, despite a shorter infection period (Table 1). A total of 11 hepatic foci were examined in 10 mice (five each from DBA/2 and AKR/N mice), and 11 cystic lesions were examined in five cotton rats. Since some lesions were too small and others were located in deeper regions not visible macroscopically, the number of histologically observed foci did not always match the number of collected liver samples. Also, the number of observed foci did not reflect the total number of *E. multilocularis* cysts present.

In mice, three foci showed inflammatory cell clusters, mainly neutrophils without larval cysts, suggesting parasitic elimination (Fig. 2A). The remaining foci displayed both unilocular and multilocular cysts surrounded by neutrophils (Figs. 2B, C). The multilocular cysts were in direct contact with each other, with internal septation observed in four foci and exogenous budding in three. Minimal neutrophil infiltration was observed in the interfollicular spaces. In cotton rats, one focus exhibited inflammatory infiltration without cyst formation, similar to that observed in the mice (Table 1). The remaining foci showed both unilocular and multilocular

cysts, each lined with a single-cell layer (Figs. 2D and E). Notably, multilocular cysts exhibited prominent neutrophil accumulation with cell debris in the intercystic spaces, whereas budding cysts had fewer surrounding neutrophils. Although eosinophils also infiltrated around the foci, their number was much lower than that of the S100A9^{+} neutrophils (Figs. 2F and G). In both species, some cysts were enclosed by a PAS-positive cuticular layer, independent of cyst type (Figs. 2H and I). No brood capsules were observed in either of the species.

Fibrotic encapsulation was present in both species, but they differed in structure (Figs. 3A and B). In mice, dense Sirius Red^{+} collagen, namely the adventitial layer, formed adjacent to the cysts (Fig. 3A'), restricting exogenous budding within the fibrotic region (Fig. 3A''). In contrast, cotton rats lacking this adventitial layer (Fig. 3B'), exhibited cyst budding beyond the fibrotic region (Fig. 3B''). Although the fibrotic layer thickness was comparable (Fig. 3C), the Sirius Red^{+} collagen area was significantly reduced in the cotton rats (Fig. 3D). Notably, despite reduced collagen, αSMA^{+} and desmin^{+} myofibroblasts were densely distributed at the cyst margins in cotton rats (Fig. 3E).

Species differences in macrophage distribution around cysts

The expression of M2 macrophage markers (CD163 and CD206) were validated in cotton rats based on their co-expression with the pan-macrophage marker Iba1 (Figs. S1A-D). In mice, CD163^{+} and CD206^{+} macrophages with irregular morphology were localized to fibrotic regions, but were rarely observed at the cyst margins (Figs. 4A and B). Similarly, in cotton rats, spindle-shaped CD163^{+} and CD206^{+} macrophages were present in fibrotic regions (Fig. 4A). Notably, cotton rats exhibited a substantial accumulation of CD206^{+} macrophages with an enlarged cytoplasm in the pericystic region (Figs. 4A and C). Within this pericystic region, large phagocytic cells containing pyknotic nuclei and eosinophilic cytoplasm were observed (Fig. 4D). These pyknotic cells were positive for ssDNA, an apoptosis marker, indicating the

presence of apoptotic cells (Fig. 4E). The number of ssDNA$^+$ cells was notably higher in the pericystic region (Fig. 4F). Furthermore, CD206$^+$ macrophages engulfed S100A9$^+$ neutrophils with pyknotic nuclei (Fig. 4G), demonstrating efferocytosis of apoptotic neutrophils by M2 macrophages.

Efferocytosis of apoptotic neutrophils promotes macrophage polarization toward the anti-inflammatory M2 phenotype, with galectin-3 playing a central role in this process (Liu et al., 2024; Zangbede et al., 2018). These macrophages are known to release factors such as TGF-β, IL-10, and VEGF (Bratton & Henson, 2011; De Lorenzo et al., 2010). In cotton rats, CD206$^+$ macrophages adjacent to the cyst periphery expressed both galectin-3 and TGF-β (Figs. 5A and B). Macrophages coexpressed CD206 and CD204 in the pericystic region (Fig. S1E), and the CD204$^+$ macrophages in this area also expressed VEGF (Fig. 5C). Notably, the CD204$^+$ macrophages beneath the cysts expressed cathepsin K and MMP9, which are collagen-degrading enzymes (Figs. 5D and E). Additionally, pericystic CD204$^+$ macrophages expressed FGF2 (Fig. 5F), a known parasite growth factor that may promote parasite development (Förster et al., 2019). In contrast, the expression of these factors was rarely observed in CD204$^+$ macrophages located in the fibrotic regions.

DISCUSSION

This study addresses the species-specific susceptibility of cotton rats to *E. multilocularis*, highlighting the distinct macrophage-driven tissue responses involved in parasite development. Compared to the inbred mouse strains commonly used in this field, cotton rats exhibit markedly accelerated cystic development, accompanied by a weaker fibrotic response, dense neutrophil infiltration around the cysts, and accumulation of CD206$^+$ macrophages at the periphery. The CD206$^+$ macrophages phagocytosed apoptotic neutrophils, suggesting a potential mechanism by which *E. multilocularis* evades host immune responses and promotes its development in

252 cotton rats.

253 Comparing tissue responses to *E. multilocularis* infection between host species with
254 different parasite developmental speeds is challenging, because tissue responses change
255 drastically during the early stages of infection (Tian et al., 2021; Wang et al., 2021). Based on
256 a previous report (Matsumoto et al., 2010), we harvested livers from cotton rats at 2 weeks post-
257 oral infection and from mice at 4 weeks. Although the number of lesions differed between the
258 two species at these time points, their macroscopic sizes were similar. Although the formation
259 of the cuticular layer was not uniform, brood capsules were consistently absent in all cysts of
260 both species. Therefore, despite differences in post-infection time points, the study was able to
261 compare tissue responses to larval cysts at a similar developmental stage.

262 Despite interspecies differences, both cotton rats and mice exhibited fibrotic encapsulation
263 of *E. multilocularis* cysts, with $CD163^+$ and $CD206^+$ macrophages localized within fibrotic
264 regions. These macrophage subsets are known mediators of hepatic fibrosis in human liver
265 diseases, such as fatty liver disease and chronic viral hepatitis (Gantzel et al., 2021; Xi et al.,
266 2021). In mice, hepatic macrophages polarize towards an M2 phenotype over time during *E.*
267 *multilocularis* infection, and experimental depletion of these cells reduces fibrosis, but
268 exacerbates disease progression (Wang et al., 2021). These findings suggest a conserved role of
269 M2 macrophages in the fibrotic response to *E. multilocularis* infection. However, species-
270 specific differences have also been observed. Cotton rats lacked the dense adventitial layers
271 observed in mice, resulting in overall reduced collagen deposition, despite infiltration of
272 numerous αSMA^+ and $desmin^+$ myofibroblasts. This attenuated fibrotic response is consistent
273 with previous reports indicating that more resistant mouse strains mount stronger fibrotic
274 reactions following *E. multilocularis* infection (Guerret et al., 1998). In addition, cotton rats
275 showed marked neutrophil accumulation near the cysts, despite rapid larval development. This
276 apparent contradiction suggests that *E. multilocularis* exploits cotton rat-specific

277 immunoregulatory pathways to evade or manipulate host defenses during cyst development.

278 In cotton rats, despite the rapid growth of *E. multilocularis*, a massive number of $S100A9^+$
279 neutrophils, rather than eosinophils, infiltrated along the cyst margin. $CD206^+$ macrophages
280 were localized adjacent to these neutrophils and phagocytosed the apoptotic cells, indicating
281 robust efferocytosis and M2 polarization in the pericystic region. Notably, *E. multilocularis*
282 oncosphere- and metacestode-derived products can induce apoptosis (Nono et al., 2012).
283 Consistent with this, numerous $ssDNA^+$ apoptotic cells were observed in the pericystic region
284 in this study. Mechanistically, neutrophil-derived S100A9 drives the M2 polarization of
285 macrophages (Mizutani et al., 2023; van Kooten et al., 2024). Additionally, efferocytosis of
286 S100A9-containing neutrophils is a well-established driver of macrophages towards M2
287 phenotype, promotes the release of various factors such as TGF-β, IL-10, and VEGF by the
288 efferocytic macrophages (Bratton & Henson, 2011; De Lorenzo et al., 2010; Liu et al., 2024).
289 Galectin-3 is essential for efferocytic clearance of neutrophils by M2 macrophages (Zangbede
290 et al., 2018). Consistent with these mechanisms, $CD206^+$ macrophages in cotton rats engulfed
291 apoptotic neutrophils and expressed Galectin-3, TGF-β, and VEGF, suggesting that
292 efferocytosis may contribute to immune evasion at the host–parasite interface. Similar immune
293 modulation has been reported in infections with *Trypanosoma cruzi* (Garrido et al., 2011),
294 *Fasciola hepatica* (Donnelly et al., 2005), and *Schistosoma japonicum* (Xu et al., 2014), where
295 M2 macrophages facilitate the parasite escape from inflammatory responses and prolong
296 infections. These findings indicate that parasite-induced apoptosis actively drives macrophages
297 toward an anti-inflammatory phenotype via efferocytosis by neutrophils, thereby creating a
298 local environment that evades immune attacks.

299 In addition to their role in promoting fibrosis, M2 macrophages also contribute to its
300 resolution (Long et al., 2023), transitioning to an anti-fibrotic phenotype and secreting matrix-
301 degrading enzymes such as matrix metalloproteinases. In cotton rats, $CD206^+$ macrophages

near larval cysts expressed cathepsin K and MMP9, also found in the epithelioid and giant multinucleated cells in cattle infected with *E. granulosus* (Díaz et al., 2000; Marco et al., 2006). Anti-*E. multilocularis* compounds, such as crocin (Liu et al., 2021), allicin (Liu et al., 2022), and asparagusic acid (Lu et al., 2024) suppress parasite growth, reduce MMP2/MMP9 expression, and increase collagen deposition. Conversely, cathepsin K deficiency exacerbates fibrosis in bleomycin-induced lung injury (Bühling et al., 2004). Our observation that $CD206^{+}$ macrophages express these enzymes, together with the attenuated fibrosis seen in cotton rats, suggests that efferocytic macrophages may promote *E. multilocularis* exogenous budding by actively degrading the surrounding collagen matrix.

Host-derived growth factors may directly contribute to *E. multilocularis* development at multiple stages. For instance, host-derived FGFs promote metacestode growth by activating parasite-specific receptors (Förster et al., 2019). In the present study, $CD204^{+}$ macrophages in the pericystic region expressed FGF2, suggesting that *E. multilocularis* exploited macrophage-derived growth factors to support its development. Additionally, systemic factors such as insulin, which is known to be elevated in cotton rats, enhance metacestode proliferation via receptor-mediated mechanisms (Hemer et al., 2014; Nakamura et al., 2019). Collectively, these findings suggest that *E. multilocularis* growth in cotton rats is facilitated by macrophage-driven collagen degradation and host-derived growth signals.

A key limitation of this study was its focus on liver histopathology at a single developmental stage of the metacestode. Species-specific susceptibility to *E. multilocularis* infection may arise earlier during oncosphere migration from the intestine or at later stages, such as protoscolex development. For instance, mouse strains differ in their larval migration efficiencies (Hayashi et al., 2021). Cotton rats also exhibited fewer inflammatory foci without cysts, suggesting limited early larval elimination. As M1 macrophages may mediate early clearance (Wang et al., 2021), identifying reliable M1 markers in cotton rats is critical for

characterizing these responses. While we focused on the liver, host factors in the extrahepatic tissues may also influence parasite development. Future studies covering multiple stages and tissues are needed to fully clarify host-parasite interactions.

Conclusion

This study established the cotton rat as a valuable model for investigating *E. multilocularis* infection and the host factors that facilitate parasite establishment. Given the expanding geographic range of *E. multilocularis* in North America and the wide distribution of cotton rats, our results highlight the potential role of this species in parasite transmission in newly endemic areas, raising important public health concerns. Cotton rats offer a powerful and biologically relevant platform for advancing alveolar echinococcosis research and developing targeted intervention strategies.

Acknowledgments

The authors declare no conflict of interest. We would like to thank Editage (www.editage.jp) for the English language editing.

REFERENCES

Bratton, D. L. & Henson, P. M. (2011). Neutrophil clearance: when the party is over, clean-up begins. Trends Immunol 32, 350–357.

Bühling, F., Röcken, C., Brasch, F., Hartig, R., Yasuda, Y., Saftig, P., Brömme, D. & Welte, T. (2004). Pivotal role of cathepsin K in lung fibrosis. Am J Pathol 164, 2203–2216.

De Lorenzo, B. H., Godoy, L. C., Novaes e Brito, R. R., Pagano, R. L., Amorim-Dias, M. A., Grosso, D. M., Lopes, J. D. & Mariano, M. (2010). Macrophage suppression following phagocytosis of apoptotic neutrophils is mediated by the S100A9 calcium-binding protein.

Immunobiology 215, 341–347.

Donnelly, S., O'Neill, S. M., Sekiya, M., Mulcahy, G. & Dalton, J. P. (2005). Thioredoxin peroxidase secreted by Fasciola hepatica induces the alternative activation of macrophages. Infect Immun 73, 166–173.

Díaz, A., Casaravilla, C., Irigoín, F., Lin, G., Previato, J. O. & Ferreira, F. (2011). Understanding the laminated layer of larval *Echinococcus* I: structure. Trends Parasitol 27, 204–213.

Díaz, A., Willis, A. C. & Sim, R. B. (2000). Expression of the proteinase specialized in bone resorption, cathepsin K, in granulomatous inflammation. Mol Med 6, 648–659.

Faith, R. E., Montgomery, C. A., Durfee, W. J., Aguilar-Cordova, E. & Wyde, P. R. (1997). The cotton rat in biomedical research. Lab Anim Sci 47, 337–345.

Förster, S., Koziol, U., Schäfer, T., Duvoisin, R., Cailliau, K., Vanderstraete, M., Dissous, C. & Brehm, K. (2019). The role of fibroblast growth factor signalling in *Echinococcus multilocularis* development and host-parasite interaction. PLoS Negl Trop Dis 13, e0006959.

Gantzel, R. H., Kjær, M. B., Laursen, T. L., Kazankov, K., George, J., Møller, H. J. & Grønbæk, H. (2021). Macrophage activation markers, soluble CD163 and mannose receptor, in liver fibrosis. Front Med 7, 615599.

Garrido, V. V., Dulgerian, L. R., Stempin, C. C. & Cerbán, F. M. (2011). The increase in mannose receptor recycling favors arginase induction and *Trypanosoma Cruzi* survival in macrophages. Int J Biol Sci 7, 1257–1272.

Guerret, S., Vuitton, D. A., Liance, M., Pater, C. & Carbillet, J. P. (1998). *Echinococcus multilocularis*: relationship between susceptibility/resistance and liver fibrogenesis in experimental mice. Parasitol Res 84, 657–667.

Hayashi, N., Kouguchi, H., Imasato, Y., Irie, T., Yagi, K., Nonaka, N. & Nakao, R. (2021). Early-phase migration dynamics of *Echinococcus multilocularis* in two mouse strains

showing different infection susceptibilities. Int J Parasitol 51, 893–898.

Hemer, S., Konrad, C., Spiliotis, M., Koziol, U., Schaack, D., Förster, S., Gelmedin, V., Stadelmann, B., Dandekar, T., Hemphill, A. & Brehm, K. (2014). Host insulin stimulates *Echinococcus multilocularis* insulin signalling pathways and larval development. BMC Biol 12, 5.

Ichii, O., Nakamura, T., Irie, T., Kouguchi, H., Nakamura, D., Nakamura, S., Sato, S., Yokoyama, K., Horino, T., Sunden, Y., Elewa, Y. & Kon, Y. (2016). Female cotton rats (*Sigmodon hispidus*) develop chronic anemia with renal inflammation and cystic changes. Histochem Cell Biol 146, 351–362.

Jiang, Y., Cai, R., Huang, Y., Zhu, L., Xiao, L., Wang, C. & Wang, L. (2024). Macrophages in organ fibrosis: from pathogenesis to therapeutic targets. Cell Death Discov 10, 487.

Kouguchi, H., Irie, T., Matsumoto, J., Nakao, R., Sugano, Y., Oku, Y. & Yagi, K. (2016). The timing of worm exclusion in dogs repeatedly infected with the cestode *Echinococcus multilocularis*. J. Helminthol 90, 766–772.

Liu, C., Fan, H., Guan, L., Ge, R. L. & Ma, L. (2021). In vivo and in vitro efficacy of crocin against *Echinococcus multilocularis*. Parasit Vectors 14, 364.

Liu, C., Fan, H., Guan, L., Ma, L. & Ge, R. L. (2022). Evaluation of allicin against alveolar echinococcosis *in vitro* and in a mouse model. Acta Parasitol 67, 79-93.

Liu, X., Ou, X., Zhang, T., Li, X., Qiao, Q., Jia, L., Xu, Z., Zhang, F., Tian, T., Lan, H., Yang, C., Kong, L. & Zhang, Z. (2024). *In situ* neutrophil apoptosis and macrophage efferocytosis mediated by Glycyrrhiza protein nanoparticles for acute inflammation therapy. J Control Release 369, 215–230.

Long, H., Lichtnekert, J., Andrassy, J., Schraml, B. U., Romagnani, P. & Anders, H. J. (2023). Macrophages and fibrosis: how resident and infiltrating mononuclear phagocytes account for organ injury, regeneration or atrophy. Front Immunol 14, 1194988.

Lu, Z., Wang, Y., Liu, C. & Fan, H. (2024). Efficacy and safety of asparagusic acid against *Echinococcus multilocularis* in vitro and in a murine infection model. Trop Med Infect Dis 9, 110.

Marco, M., Baz, A., Fernandez, C., Gonzalez, G., Hellman, U., Salinas, G. & Nieto, A. (2006). A relevant enzyme in granulomatous reaction, active matrix metalloproteinase-9, found in bovine *Echinococcus granulosus* hydatid cyst wall and fluid. Parasitol Res 100, 131–139.

Massolo, A., Liccioli, S., Budke, C. & Klein, C. (2014). *Echinococcus multilocularis* in North America: the great unknown. Parasite 21, 73.

Matsumoto, J., Kouguchi, H., Oku, Y. & Yagi, K. (2010). Primary alveolar echinococcosis: Course of larval development and antibody responses in intermediate host rodents with different genetic backgrounds after oral infection with eggs of *Echinococcus multilocularis*. Parasitol Int 59, 435–444.

Mizutani, T., Ano, T., Tsuruyama, Y., Mizuta, S., Takemoto, K., Ouchi, Y., Morita, D., Kitano, S., Miyachi, H., Tsuruyama, T., Fujiwara, N. & Sugita, M. (2023). Neutrophil S100A9 supports M2 macrophage niche formation in granulomas. iScience 26, 106081.

Nakamura, T., Ichii, O., Irie, T., Kouguchi, H., Sotozaki, K., Chihara, M., Sunden, Y., Nagasaki, K., Tatsumi, O., Elewa, Y. & Kon, Y. (2019). Cotton rat (*Sigmodon hispidus*) develops metabolic disorders associated with visceral adipose inflammation and fatty pancreas without obesity. Cell Tissue Res 375, 483–492.

Nakao, R., Kameda, Y., Kouguchi, H., Matsumoto, J., Dang, Z., Simon, A., Torigoe, D., Sasaki, N., Oku, Y., Sugimoto, C., Agui, T. & Yagi, K. (2011). Identification of genetic loci affecting the establishment and development of *Echinococcus multilocularis* larvae in mice. Int J Parasitol 41, 1121–1128.

Nakaya, K., Nakao, M. & Ito, A. (1997). *Echinococcus multilocularis*: Mouse strain difference in hydatid development. J Helminthol 71, 53–56.

Nono, J. K., Pletinckx, K., Lutz, M. B. & Brehm, K. (2012). Excretory/secretory-products of *Echinococcus multilocularis* larvae induce apoptosis and tolerogenic properties in dendritic cells *in vitro*. PLoS Negl Trop Dis 6, e1516.

Reuben, J. M., Tanner, C. E. & Rau, M. E. (1978). Immunoprophylaxis with BCG of experimental *Echinococcus multilocularis* infections. Infect Immun 21, 135–139.

Sakamoto, T. & Sugimura, M. (1970). Studies on echinococcosis. 23. Electron microscopical observations on histogenesis of larval *Echinococcus multilocularis*. Jpn J Vet Res 18, 131–144.

Tian, F., Jiang, T., Qi, X., Zhao, Z., Li, B., Aibibula, M., Min, H., Zhang, J., Liu, Y. & Ma, X. (2021). Role of cytokines on the progression of liver fibrosis in mice infected with *Echinococcus multilocularis*. Infect Drug Resist 14, 5651–5660.

Torgerson, P. R., Keller, K., Magnotta, M. & Ragland, N. (2010). The global burden of alveolar echinococcosis. PLoS Negl Trop Dis 4, e722.

van Kooten, N. J. T., Blom, A. B., Teunissen van Manen, I. J., Theeuwes, W. F., Roth, J., Gorris, M. A. J., Walgreen, B., Sloetjes, A. W., Helsen, M. M., Vitters, E. L., van Lent, P. L. E. M., Koëter, S., van der Kraan, P. M., Vogl, T. & van den Bosch, M. H. J. (2024). S100A8/A9 drives monocytes towards M2-like macrophage differentiation and associates with M2-like macrophages in osteoarthritic synovium. Rheumatology 64, 332–343.

Vuitton, D. A., Zhang, S. L., Yang, Y., Godot, V., Beurton, I., Mantion, G. & Bresson-Hadni, S. (2006). Survival strategy of *Echinococcus multilocularis* in the human host. Parasitol Int 55, S51–S55.

Wang, H., Zhang, C. S., Fang, B. B., Hou, J., Li, W. D., Li, Z. D., Li, L., Bi, X. J., Li, L., Abulizi, A., Shao, Y. M., Lin, R. Y. & Wen, H. (2021). Dual role of hepatic macrophages in the establishment of the *Echinococcus multilocularis* metacestode in mice. Front Immunol 11, 600635.

Wynn, T. A. & Vannella, K. M. (2016). Macrophages in tissue repair, regeneration, and fibrosis. Immunity 44, 450–462.

Xi, S., Zheng, X., Li, X., Jiang, Y., Wu, Y., Gong, J., Jie, Y., Li, Z., Cao, J., Sha, L., Zhang, M. & Chong, Y. (2021). Activated hepatic stellate cells induce infiltration and formation of $CD163^{+}$ macrophages via CCL2/CCR2 pathway. Front Med 8, 627927.

Xu, J., Zhang, H., Chen, L., Zhang, D., Ji, M., Wu, H. & Wu, G. (2014). *Schistosoma japonicum* infection induces macrophage polarization. J Biomed Res 28, 299-308.

Quenum Zangbede, F. O., Chauhan, A., Sharma, J. & Mishra, B. B. (2018). Galectin-3 in M2 macrophages plays a protective role in resolution of neuropathology in brain parasitic infection by regulating neutrophil turnover. J Neurosci 38, 6737–6750.

FIGURE LEGENDS

Fig. 1 Macroscopic views of the livers infected with larval *E. multilocularis*.

Livers of inbred mouse strains AKR/N (A), DBA/2 (B), and cotton rats (C), orally inoculated with 200 eggs of the parasite, observed at 4 weeks (mice) and 2 weeks (cotton rats) after infection. Whitish dots on the liver represent established larval cysts. More lesions were found in cotton rats than in susceptible mouse strains despite their similar diameters. The boxed area is magnified in the lower left.

Fig. 2 Developmental stage of *E. multilocularis* and the tissue reaction in the infected liver.

(A-C) Liver sections of mice, showing infiltration foci without larval cysts (A), uniocular cysts (B), and multilocular cysts with internal septation (C). Neutrophils surrounding the cysts, but did not infiltrate into inter-cystic spaces. (D and E) Liver sections of cotton rats, showing multilocular cysts with internal septation (D) and those with exogenous budding (E). numerous neutrophils infiltrated in the inter-cystic region. HE staining. (F and G) Luna staining and

immunohistochemistry for S100A9, highlighting eosinophils (F) and neutrophils (G), respectively. Eosinophil granules are stained red. (H and I) PAS staining of mice (H) and cotton rats (I), showing a part of the cysts produced cuticular layers. C: cysts, F: fibrotic region, L: uninfected liver, P: pericystic region. Asterisks indicate PAS^+ cysts.

Fig. 3 Different development of fibrosis around the cysts.

(A-A'') Liver sections of mice showing developed adventitial layers (A') and budding cysts that do not exceed the fibrotic regions (A''). Arrows indicate adventitial layers. (B) Liver sections from cotton rats showing a lack of adventitial layers (B') and budding cysts penetrating the fibrotic regions (B'). Picrosirius red staining. (C and D) Comparison of the thickness of the fibrotic region (C) and ratio of Sirius red^+ area to fibrotic area (D). $^{**}P < 0.01$, by Student's *t*-test. (E) Immunohistochemistry for αSMA and desmin at the periphery of the cysts, indicating numerous infiltrations of myofibroblast despite the lack of adventitial layers. C: cysts; F: fibrotic region; L: uninfected liver; P: pericystic region.

Fig. 4 Different distribution of M2 macrophages around the cysts.

(A) Immunohistochemistry for CD163 and CD206 in the liver sections of mice and cotton rats. (B and C) Quantification of infiltrating macrophages in mice (B) and cotton rats (C). (D) Phagocytosis of apoptotic neutrophils in the pericystic region of cotton rat. HE staining. (E) Immunohistochemistry for apoptosis marker, ssDNA in cotton rat. (F) quantification of $ssDNA^+$ cells around the cyst in the liver sections. (G) Immunofluorescence for CD206 and S100A9, markers for M2 macrophages and neutrophils, respectively. $^{*}P < 0.05$, $^{**}P < 0.01$, $^{***}P < 0.001$, by one-way ANOVA with Tukey's multiple comparisons test. $\#P < 0.05$, by Student's *t*-test. C: cysts, F: fibrotic region, L: uninfected liver, P: pericystic region. Arrows indicate phagocytosed cells.

Fig. 5 Efferocytosis- and cystic growth-associated markers in M2 macrophages around the cysts.

(A-C) Immunofluorescence for M2 macrophage markers (CD204 and CD206) and efferocytsis-associated molecules (Galectin-3, TGF-β, and VEGF). (D and E) Immunofluorescence for CD204 and molecules associating degradation of collagen fibers (cathepsin K and MMP9). (F) Immunofluorescence for CD204 and FGF2, a known growth factor for both hosts and parasites. C: cysts, F: fibrotic region, P: pericystic region, F: fibrotic region. Arrows indicate double-positive cells.

Table 1. Growth stage of *Echinococcus multilocularis*.

	Mice (DBA/2 and AKR/N)	Cotton rats
Infiltration foci without larval cyst	3	1
Uniocular cyst	1*	0
Multiocular cyst, internal septation	4*	2*
Multiocular cyst, exogenous budding	3*	8*
Brood capsule formation	0	0
Total foci	11	11

Stages were categorized according to the criteria of Sakamoto et al. (1970), with minor modifications. Since internal septation was consistently observed in cysts with exogenous budding, but not all septated cysts exhibited budding, we defined exogenous budding to represent a more developed stage in this study. * Part of the cyst surrounded by PAS+ cuticular layers.

Fig. 1

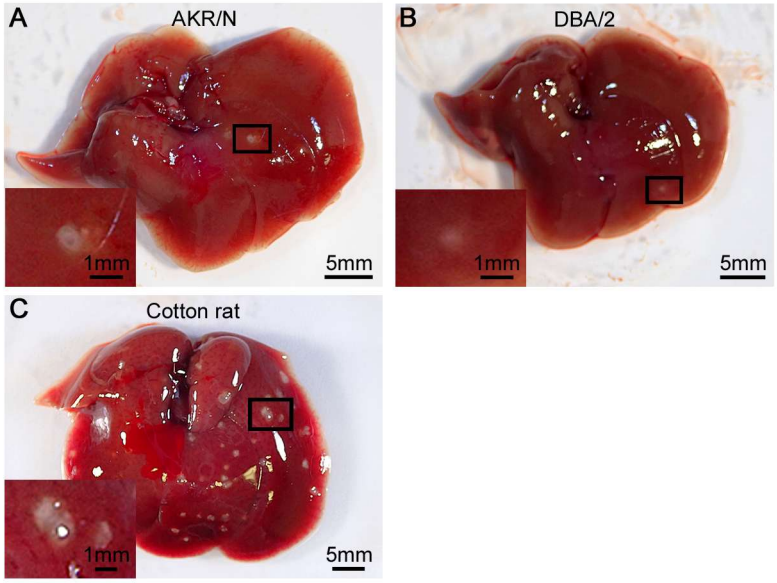

Fig. 2

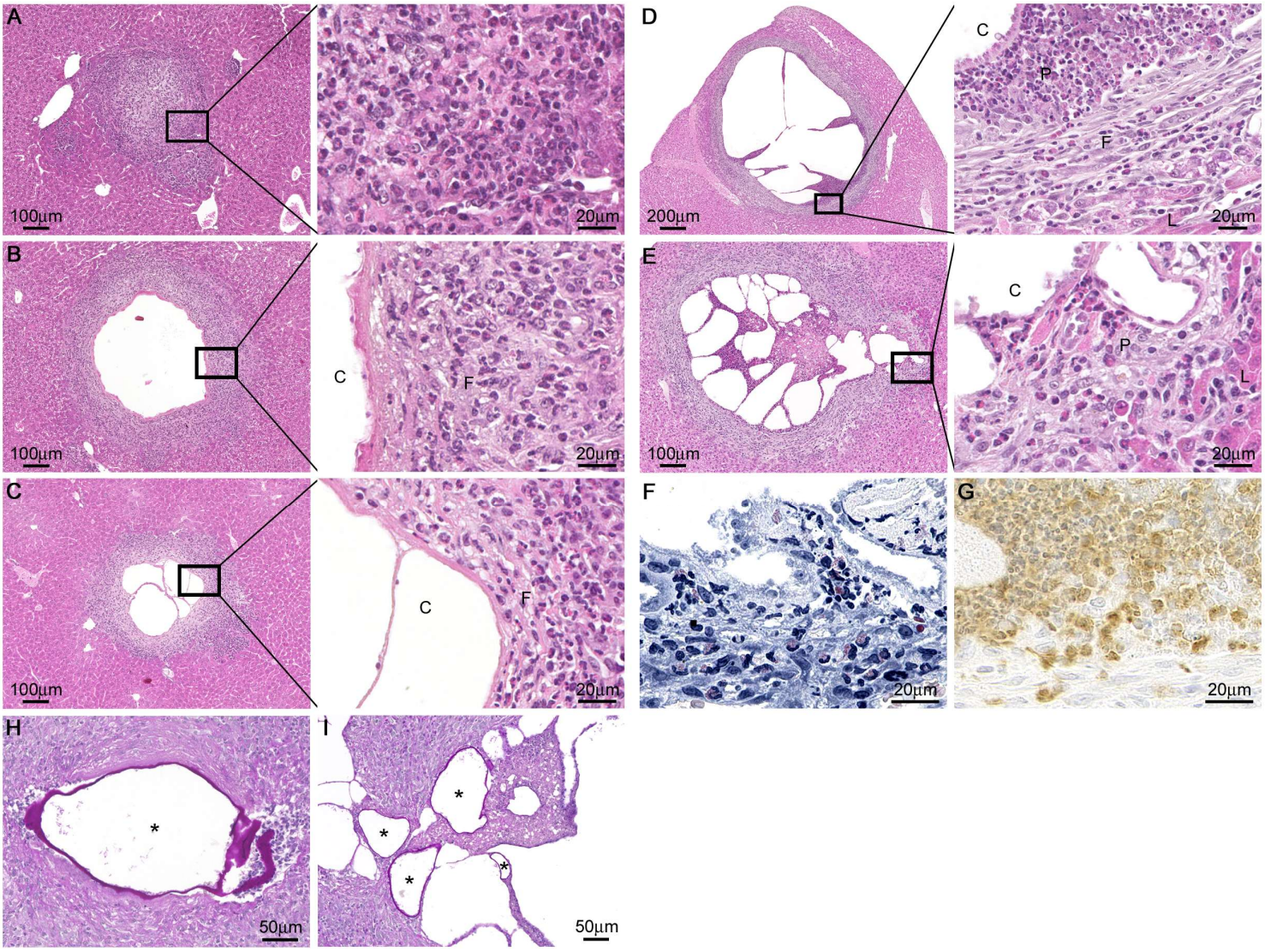
A
100μm
20μm
B
100μm
C
F
20μm
C
100μm
C
F
20μm
H
*
50μm
I
*
*
*
*
50μm
D
200μm
C
P
F
L
20μm
E
100μm
C
P
L
20μm
F
20μm
G
20μm

Fig. 3

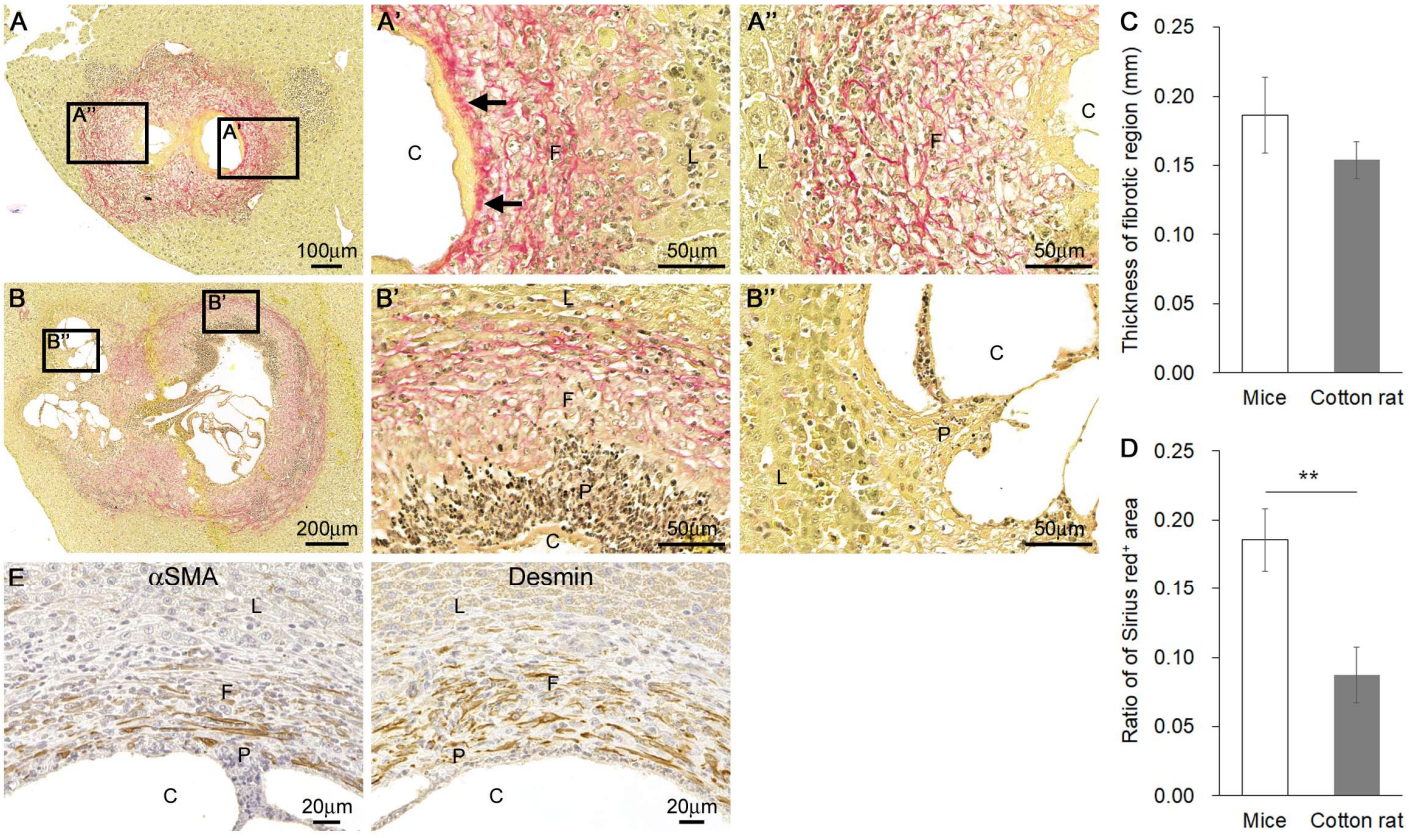
A
A''
A'
100μm
A'
C
F
L
50μm
A''
C
L
F
50μm
B
B'
B''
200μm
B'
L
F
P
C
50μm
B''
C
P
L
50μm
E
αSMA
L
F
P
C
20μm
Desmin
L
F
P
C
20μm
C
Thickness of fibrotic region (mm)
0.25
0.20
0.15
0.10
0.05
0.00
Mice
Cotton rat
D
Ratio of of Sirius red+ area
**
0.25
0.20
0.15
0.10
0.05
0.00
Mice
Cotton rat

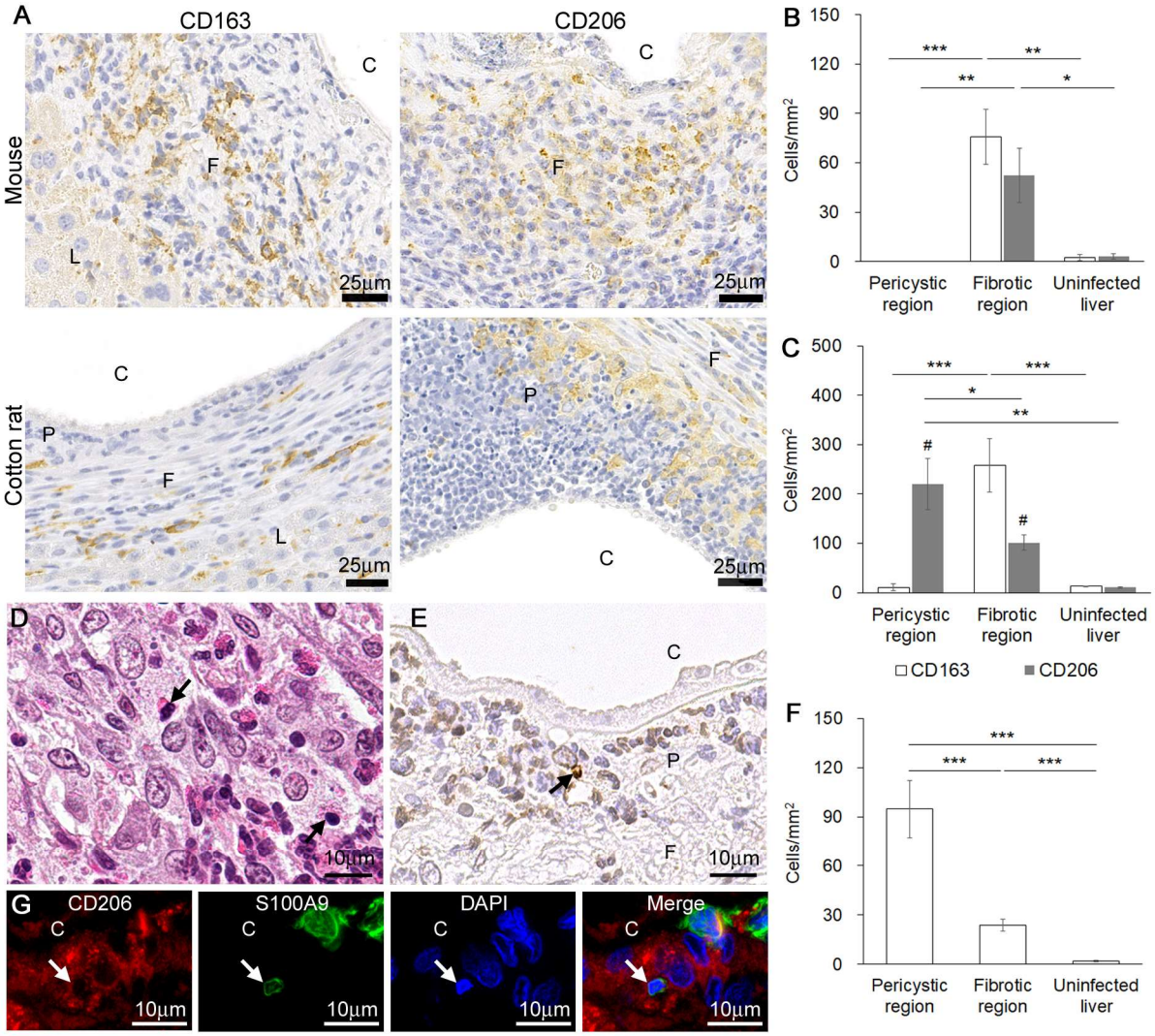
A
CD163
CD206
Mouse
Cotton rat
C
F
L
P
25µm
B
Cells/mm²
Pericystic region
Fibrotic region
Uninfected liver
C
CD163
CD206
D
E
10µm
G
CD206
S100A9
DAPI
Merge

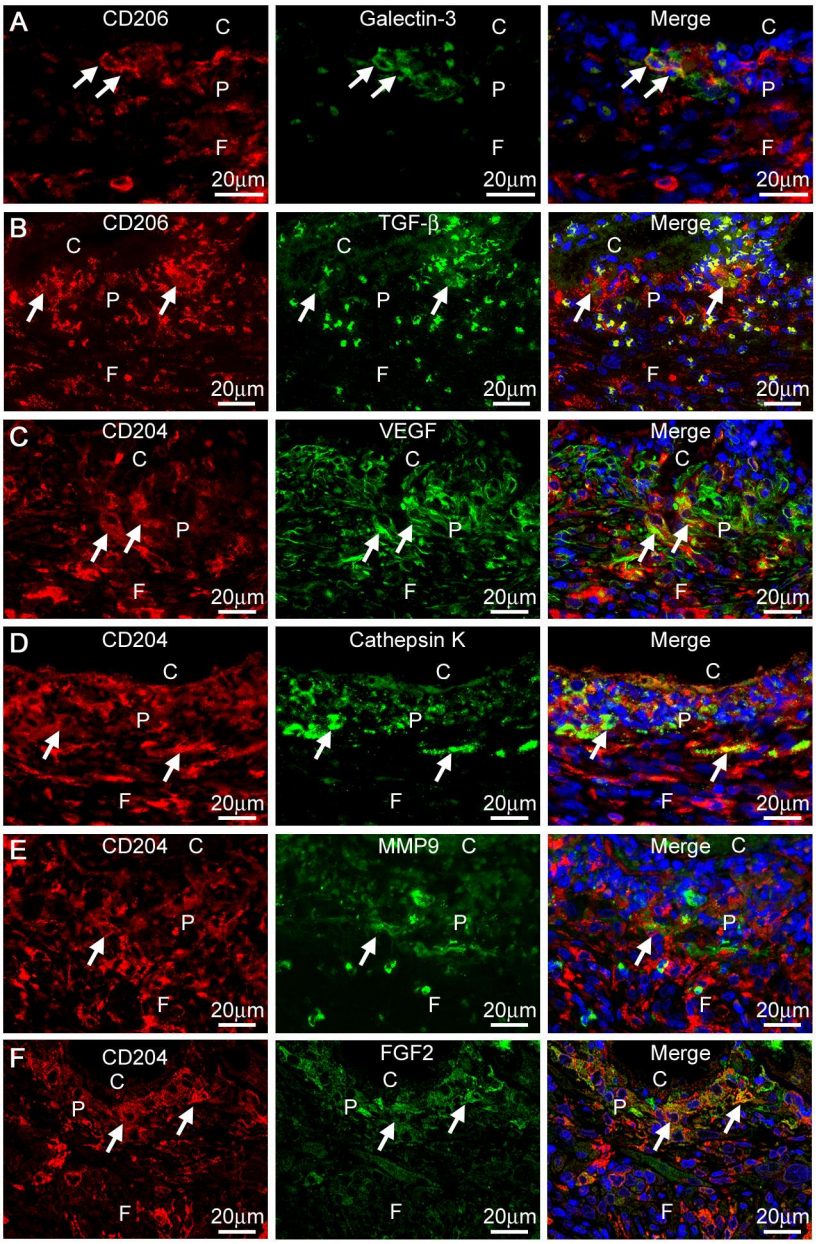
A
CD206
Galectin-3
Merge
B
CD206
TGF-β
Merge
C
CD204
VEGF
Merge
D
CD204
Cathepsin K
Merge
E
CD204
MMP9
Merge
F
CD204
FGF2
Merge
C
P
F
20μm

Supplemental Table 1. List of antibodies.

Antibody (Product #)	Source	Dilution	Antigen retrieval
Goat anti-Iba1, polyclonal (011-27991)	Fujifilm Wako (Osaka, Japan)	1:500	CB, 105 °C, 20 min
Mouse-anti iNOS, monoclonal (ab49999)	Abcam (Cambridge, UK)	1:500	IS, 105 °C, 20 min
Rabbit anti-Arginase-1, monoclonal (93668)	Cell Signaling (MA, USA)	1:500	CB, 105 °C, 20 min
Rabbit anti-CD163, monoclonal (ab182422)	Abcam	1:1000	CB, 105 °C, 20 min
Mouse anti-CD204, monoclonal (KMU-MA01A)	Cosmo Bio (Tokyo, Japan)	1:300	CB, 105 °C, 20 min
Rabbit anti-CD206, monoclonal (24595)	Cell Signaling	1:500	CB, 105 °C, 20 min
Mouse anti-αSMA, monoclonal (Z2066MT)	Zeta (CA, USA)	1:500	CB, 105 °C, 20 min
Mouse anti-desmin, monoclonal (D1033)	Sigma-Aldrich (MO, USA)	1:1000	CB, 105 °C, 20 min
Rabbit anti-ssDNA, polyclonal (18731)	IBL (Gunma, Japan)	1:5000	Not done
Mouse anti-S100A9, monoclonal (MA1-81381)	Thermo Fisher (MA, USA)	1:1000	IS, 105 °C, 20 min
Mouse anti-galectin-3, monoclonal (sc-32790)	Santacruz (TX, USA)	1:300	CB, 105 °C, 20 min
Mouse anti-TGF-β, monoclonal (MCA797)	Bio-Rad (CA, USA)	1:500	IS, 105 °C, 20 min
Rabbit anti-VEGFA, monoclonal (ab52917)	Abcam	1:300	CB, 105 °C, 20 min
Rabbit anti-Cathepsin K, polyclonal (ab19027)	Abcam	1:300	CB, 105 °C, 20 min
Rabbit anti-MMP9, multiclonal (ab283575)	Abcam	1:1000	CB, 105 °C, 20 min
Rabbit anti-FGF2, polyclonal (PA5-116495)	Thermo Fisher	1:1000	CB, 105 °C, 20 min
Biotin-labeled goat anti-mouse IgG (1030-08)	SouthernBiotech (AL, USA)	1:200	–
Biotin-labeled goat anti-rabbit IgG (424032)	Nichirei (Tokyo, Japan)	RTU	–
AF 488-labeled donkey anti-mouse IgG (A32766)	Life Technologies (CA, USA)	1:1000	–
AF 546-labeled donkey anti-mouse IgG (A10036)	Life Technologies	1:1000	–
AF 488-labeled donkey anti-rabbit IgG (A32790)	Thermo Fisher	1:1000	–
AF 594-labeled donkey anti-rabbit IgG (A-21207)	Thermo Fisher	1:1000	–
AF 488-labeled donkey anti-goat IgG (A32814)	Thermo Fisher	1:1000	–

CB, 0.01 M citrate buffer (pH 6.0); IS, 0.05 % sodium citraconate solution (Immunosaver®, Nisshin EM, Tokyo, Japan); AF, Alexa Fluor.

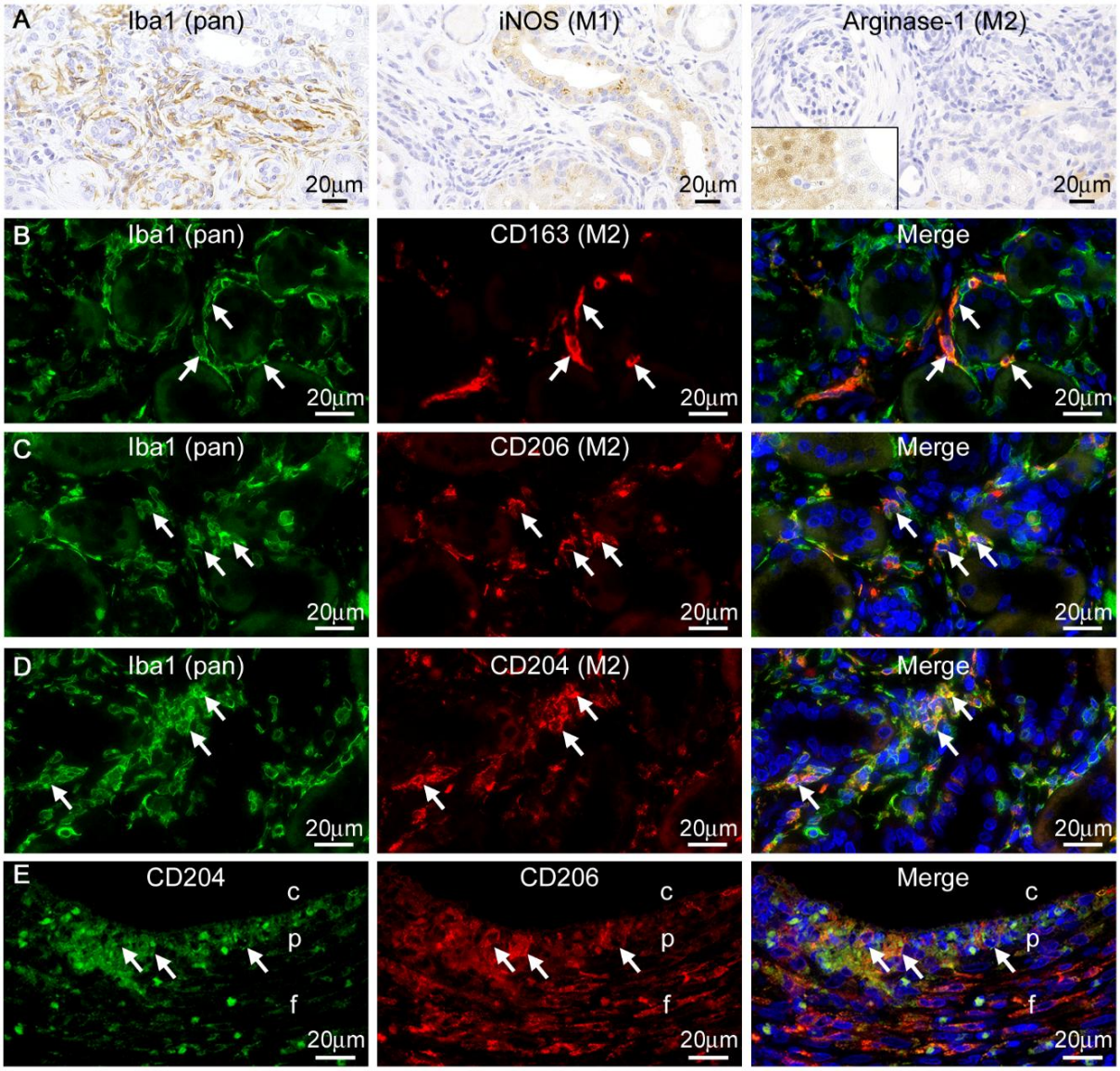

Supplemental Fig. 1 Macrophage-associated markers in cotton rats.

(A) In fibrotic kidney lesions of cotton rats, Iba1$^+$ cells were abundant in the stroma, while iNOS and arginase-1, markers of M1 and M2 macrophages in mice, were not detected. The lower left panel of Arginase-1 shows the liver sections. (B-D) CD163, CD204, and CD206 were detected in stromal cells and co-localized with Iba1, supporting their use as M2 macrophage markers in cotton rats. These markers were used for subsequent analyses in both cotton rats and mice. (E) In liver sections infected with *Echinococcus multilocularis*, macrophages co-expressed CD206 and CD204 in the pericystic retion. Arrows indicate double-positive cells. C: cysts; F: fibrotic region; P: pericystic region.